Published in final edited form as:
J Neural Eng. 2014 October ; 11(5): 056023. doi:10.1088/1741-2560/11/5/056023.

Controllable pulse parameter transcranial magnetic stimulator with enhanced circuit topology and pulse shaping

Angel V Peterchev[1,2,3], **Kevin D'Ostilio**[4,5], **John C Rothwell**[5], and **David L Murphy**[1]

Angel V Peterchev: angel.peterchev@duke.edu

[1]Department of Psychiatry and Behavioral Sciences, Duke University, Durham, NC, USA

[2]Department of Biomedical Engineering, Duke University, Durham, NC, USA

[3]Department of Electrical and Computer Engineering, Duke University, Durham, NC, USA

[4]Cyclotron Research Centre, University of Liege, Belgium

[5]Institute of Neurology, University College London, London, UK

Abstract

Objective—This work aims at flexible and practical pulse parameter control in transcranial magnetic stimulation (TMS), which is currently very limited in commercial devices.

Approach—We present a third generation controllable pulse parameter device (cTMS3) that uses a novel circuit topology with two energy-storage capacitors. It incorporates several implementation and functionality advantages over conventional TMS devices and other devices with advanced pulse shape control. cTMS3 generates lower internal voltage differences and is implemented with transistors with lower voltage rating than prior cTMS devices.

Main results—cTMS3 provides more flexible pulse shaping since the circuit topology allows four coil-voltage levels during a pulse, including approximately zero voltage. The near-zero coil voltage enables snubbing of the ringing at the end of the pulse without the need for a separate active snubber circuit. cTMS3 can generate powerful rapid pulse sequences (<10 ms inter pulse interval) by increasing the width of each subsequent pulse and utilizing the large capacitor energy storage, allowing the implementation of paradigms such as paired-pulse and quadripulse TMS with a single pulse generation circuit. cTMS3 can also generate theta (50 Hz) burst stimulation with predominantly unidirectional electric field pulses. The cTMS3 device functionality and output strength are illustrated with electrical output measurements as well as a study of the effect of pulse width and polarity on the active motor threshold in 10 healthy volunteers.

Significance—The cTMS3 features could extend the utility of TMS as a research, diagnostic, and therapeutic tool.

Keywords

transcranial magnetic stimulation; circuit; pulse shape; control; motor threshold; pulse width; directionality

Correspondence to: Angel V Peterchev, angel.peterchev@duke.edu.

K.D'O. and D.L.M. have no relevant financial disclosures.

1. Introduction

Transcranial magnetic stimulation (TMS) involves the delivery of brief, high-strength magnetic pulses to the brain to induce an electric field that modulates neural activity. TMS devices consist of a coil that is placed on the subject's head and a pulse generator that supplies high current pulses to the coil [1]. TMS and repetitive TMS (rTMS) are used as a non-invasive tool for studying the brain [2, 3, 4], an approved treatment for depression, and an investigational treatment for other psychiatric and neurological disorders [5, 6, 7, 8].

Commercially available TMS devices induce damped cosine electric field pulses, with non-existent or very limited control over the pulse shape parameters [9, 10, 11]. These conventional devices deploy a pulse generator circuit consisting essentially of an energy storage capacitor and a thyristor switch that can be triggered to discharge the capacitor into the stimulation coil but cannot be controllably turned off to shape the pulse. More flexible control of the pulse shape could potentially enable a host of research and clinical applications that are not feasible with available TMS devices, including expanded characterization of neural properties, more selective targeting of neural populations, enhanced neuromodulation effectiveness and reproducibility, reduced energy use and coil heating, as well as mitigation of pulse sensation and sound [12, 13, 11, 14, 15, 16] (see also Sec. 5).

Addressing this need, we have developed a family of TMS devices with controllable pulse parameters (cTMS) including low repetition rate TMS (cTMS1) [13] and high rate rTMS (cTMS2) [14]. cTMS1 uses a large energy storage capacitor and a single insulated gate bipolar transistor (IGBT) switch to enable pulse width control. cTMS2 deploys two capacitors and two IGBTs to extend the controllable coil voltage levels from one to two, and to provide efficient high rate rTMS operation; it requires an active snubbing circuit to suppress ringing at the end of each pulse. With these devices we demonstrated adjustment of the number, polarity, duration, and amplitude of the electric field pulse phases; reduction of power consumption and coil heating; and motor cortex stimulation in non-human primates and humans [13, 14, 15]. Another device that aims to improve the adjustability of the pulse shape, flexTMS, uses four IGBT switches, forming an H-bridge, to connect the coil to a single energy storage capacitor [17]. However, the flexTMS device has limitations including a single controllable coil voltage level due to the use of only one energy storage capacitor, restricted pulse width control due to the relatively small energy storage capacitor (66 μF—approximately an order of magnitude smaller than the capacitors in the cTMS devices), and large ringing artifacts in the pulses. Magnetic stimulation devices that potentially allow even greater pulse shaping flexibility have so far been demonstrated only at low pulse energies that are well below the range used for TMS [18, 19].

In this paper we present the design of a novel cTMS device (cTMS3) and demonstrate its functionality with electrical measurements of its output and with a first-in-human study. cTMS3 uses a novel circuit topology that incorporates several implementation and functionality advantages over previous cTMS and other TMS devices, including lower transistor voltages, more flexible pulse shaping, and intrinsic pulse snubbing capabilities.

We demonstrate the capability of the cTMS device to generate powerful, rapid pulse sequences such as theta burst stimulation, paired pulses, and quadripulses with predominantly unidirectional electric fields that are not possible with conventional TMS devices with a single pulse generation circuit. As an illustration of the application of cTMS3, we present motor threshold strength–duration curves from 10 human subjects. This work was previously presented in part in conference proceedings [20, 21, 22].

2. Device Design

2.1. Circuit Topology

Figure 1 shows a diagram of the key circuit elements of the cTMS3 device. The two terminals of the stimulation coil L, V_{x1} and V_{x2}, are driven by two half-bridge circuits connected to energy-storage capacitors C_{11} and C_{21} that are charged to voltages V_{C11} and V_{C21}, respectively. The half-bridges comprise current-bidirectional switches Q_{11}/D_{11}, Q_{12}/D_{12}, Q_{21}/D_{21}, and Q_{22}/D_{22}, which are implemented with insulated-gate bipolar transistor (IGBT) modules incorporating freewheeling diodes. Resistor R_1 sets the dc bias of the coil to earth ground for safety.

This topology allows four different voltages, $V_L = \{ V_{C11}, -V_{C21}, V_{C11} - V_{C21}, 0\}$ to be imposed on the coil during a pulse. Consequently, the electric field E induced by the coil can assume four levels, proportional to V_L. Of these, the $V_L = V_{C11}$ and $V_L = -V_{C21}$ levels correspond to those available in the cTMS2 device in which the two energy-storage capacitors are charged to opposite polarities, one terminal of the stimulation coil is grounded, and the other coil terminal is switched between the two capacitors with a single half-bridge [14]. The $V_L = V_{C11} - V_{C21}$ and $V_L = 0$ levels are unique to the novel cTMS3 topology. The coil voltage also determines the rate of change of the coil current I_L. Therefore, I_L can be ramped up and down with positive and negative V_L, respectively, or held constant with $V_L = 0$.

The active semiconductor switches are potentially the most expensive individual components in the cTMS device. In the proposed topology in figure 1 the off-state voltage in each half-bridge corresponds to the voltage of the respective energy-storage capacitor, V_{C11} and V_{C21}. Thus, the voltage ratings of the switches are lower than those in the cTMS2 device where the two switches are exposed to the sum of the two capacitor voltages [14]. Of course, for both devices, the switch voltages exceed the respective capacitor voltages during switching transients that cause voltage spikes and consequently require snubbers and a safety margin in the selection of IGBT module voltage rating (see also Sec. 2.2). For pulsed operation as in TMS, the switch current can exceed the dc rating of the IGBT module [13, 14, 23]. Even though the proposed topology uses four switches whereas cTMS2 uses only two switches, the former may be advantageous since the price of semiconductors increases rapidly and availability decreases at high voltages where production volumes are lower, motivating the use of switches with lower voltage ratings.

2.2. Pulse Snubbing

2.2.1. Passive IGBT Snubbing—Using snubbers to limit potentially damaging voltages and currents in semiconductors during switching is critical in pulsed circuits. Two types of

IGBT snubbers are incorporated in the design. First, the snubbers consisting of C_{i3}–C_{i6} and R_{i1}–R_{i2} serve the dual purpose of taking over a portion of the IGBT current during turn-off and suppressing voltage spikes across the IGBT collector–emitter due to parasitic inductances [13, 14, 24, 25]. These snubbers are connected to V_{xi} and consequently experience switching between V_{Ci1} and 0 voltage during pulse generation, potentially contributing significant CV^2 losses. Therefore, capacitances C_{i3}–C_{i6} should be kept at the minimum required for the IGBT snubbing. Second, voltage spikes resulting from stray inductance in the energy-storage capacitors and their wiring is additionally suppressed by the snubbers consisting of C_{i2}, R_{i3}, and D_{i3} [13, 26]. These snubbers are connected between V_{Ci1} and V_{COMi}, and consequently see much less voltage change than the snubbers connected to V_{xi}, resulting in smaller losses.

To reduce switching losses and the energy handled by the snubbers, parasitic inductances around the loop formed by the energy-storage capacitor, C_{i1}, and the two IGBT switches, Q_{i1} and Q_{i2}, within each half-bridge module in figure 1 have to be minimized. In contrast, parasitic inductance between the two half-bridges is in series with the coil L which dominates the inductance, and thus does not contribute to switching losses and voltage spikes. Nevertheless, the inductance between the two half-bridges acts as a voltage divider with the coil, and should therefore be kept low for good energy transfer to the coil.

2.2.2. Active Coil Snubbing—At the end of a TMS pulse, the snubber capacitance across the IGBT collector–emitter rings with the coil [14]. For example, at the end of a positive current pulse, the coil current I_L decays to zero, switching node V_{x1} is at ground potential, and switching node V_{x2} is at potential V_{C21}. Thus, there is voltage of $V_L = -V_{C21}$ across the coil. Consequently, current $I_L < 0$ builds up in the coil. The coil current starts to discharge the capacitance at node V_{x2} and charge the capacitance at node V_{x1}. To suppress the undesirable electric field oscillation that would result from the exchange of energy between the switching nodes' capacitances and the coil, the coil current has to be forced to zero by applying relatively small voltages to the coil. The cTMS3 topology in figure 1 has the advantage that it allows $V_L \approx 0$ to be applied to the coil, in contrast to the cTMS2 device where a separate active snubber circuit is required [14].

In the example above, since the current flowing in the coil is negative, diode D_{22} will turn on when node V_{x2} reaches ground (more precisely one diode voltage drop below ground). By turning on switch Q_{12} at or before the end of the TMS pulse, node V_{x1} will be held at ground as well, resulting in $V_L \approx 0$. Thus, the coil voltage and, hence, electric field ringing at the end of the pulse would be suppressed. In that case, the energy stored in the coil will gradually dissipate as the coil current flows through the intrinsic resistance of the coil and switches Q_{12} and D_{22}. Since these resistances are very small, as necessary for low conduction losses during the main pulse, the decay of the coil current will be relatively slow. For example, for typical $L = 16$ μH and total coil series resistance $r = 25$ mΩ, the current decay time constant is $L/r = 640$ μs—much longer than a typical TMS pulse. Furthermore, since the switch on-resistance is typically an order of magnitude lower than the coil resistance, the majority of the residual energy will be dissipated in the coil, which may contribute undesirable additional coil heating.

Therefore, it may be advantageous to allow a higher positive voltage on the coil to speed up the decay of the residual coil current. One way to accomplish this is to put switch Q_{12} in a high resistance mode. However, since conventional IGBT gate drivers generate only two voltage levels, corresponding to the IGBT being fully on or fully off, the IGBT cannot be operated in the high output resistance region corresponding to a gate voltage near threshold (~ 6 V). Nevertheless, by switching the gate driver rapidly between the on and off states, the IGBT can provide, on average, an output resistance that is controllable by the IGBT switching parameters.

For TMS pulses ending with a negative current phase, the same principle can be applied to suppress ringing at the pulse end, except that in this case switch Q_{22} should be pulsed instead of switch Q_{12}.

2.3. Device Implementation

We constructed a cTMS3 device based on the circuit in figure 1 with maximum capacitor voltages of $V_{C11} = 2.6$ kV and $V_{C21} = 1.0$ kV, and maximum coil current of $|I_L| = 6$ kA. Table 1 gives the key circuit components used in the implementation. Considerations for their selection are similar to those for prior cTMS devices [13, 14], with cTMS3 specific highlights discussed below.

Due to the lower voltage seen by each switch (see Sec. 2.1), cTMS3 uses 3300 V IGBT modules in contrast to prior cTMS devices that used 4500 V IGBT modules [13, 14]. On the other hand, the current rating of the cTMS3 IGBT modules is higher (1200 A versus 600 A or 900 A) to provide low total on-state voltage drop across the two switches in series with the coil. The IGBT gate drivers are based on a commercial module that was configured to have on-state voltage of $V_{GE} = 20$ V to provide low IGBT resistance, and off-state voltage of $V_{GE} = -10$ V to ensure robust IGBT turn-off. The output impedance of the gate driver is $R_G = 11\ \Omega$ for relatively slow turn-on transition to limit the current transient associated with discharging the snubber capacitors, and $R_G = 1\ \Omega$ for fast turn-off to provide rapid transfer of the IGBT current to the snubbers in order to protect the IGBTs from high instantaneous power dissipation and current hot spots [24, 25, 26].

Each of the two energy storage capacitors with the corresponding switch half-bridge was assembled on a 51 cm × 40 cm × 3.2 mm high-strength aluminum plate that doubles as a heat sink for the IGBTs. The components and wiring were laid out so as to minimize the parasitic inductance around the loop. Specifically, the IGBT modules and energy-storage capacitors were interconnected with three independent, parallel pairs of 10 AWG, 15 kV wire (P/N 391045, Manhattan Dearborn). The snubbers were mounted on top of the IGBT modules. The two half-bridges were positioned one on top of the other to provide a low inductance connection among them and the coil. The energy storage capacitors were charged with off-the-self high-voltage power supplies.

The system was controlled with a commercial compact reconfigurable I/O system (cRIO, National Instruments, USA). Interface between the cRIO and the power circuits was provided by custom electronics. The cRIO was programmed via a personal computer running LabVIEW (National Instruments) which also provided graphical user interface. The

energy-storage capacitor voltages and the coil current were measured by the controller using the power supplies' voltage sensing outputs and a custom Rogowski coil, respectively [27, 28]. The controller also monitored the temperature of the stimulation coil, IGBT modules, energy-storage capacitors, and capacitor discharge resistors.

3. Experimental Methods

3.1. Electrical Measurements

The electric field, E, was measured with a single-turn search coil fixed in front of the TMS coil [14]. The coil current, I_L, was measured with an external Rogowski current sensor (CWT30B, PEM, UK) that was clipped around the V_{x2} terminal of the coil. The Rogowski current sensor is insulated, lossless, and high-bandwidth [27, 28]. However, the sensed current waveform can be distorted by capacitive coupling to the TMS coil terminals which undergo large, rapid voltage swings during switching. Therefore, small deviations in the Rogowski current sensor output can occur after switching of the V_{x2} node. The E and I_L measurements were recorded with a digitizing oscilloscope.

3.2. Neural Membrane Voltage Model

To compare the neurostimulation strength of various TMS pulses, the neural membrane voltage change resulting from TMS, ΔV_m, was estimated by applying a first-order low-pass filter to the electric field waveform E [12, 29, 13, 14]. A larger ΔV_m magnitude signifies stronger neural stimulation. This approach is predicated on modeling the neural membrane as a leaky integrator [30]. The filter time constant can be estimated empirically from dose–response data, such as strength–duration curves for motor cortex activation [12, 13, 15]. We used a time constant of 196 μs based on motor threshold data obtained with the cTMS1 device [15]. The first-order low-pass filter was implemented with the filter function in MATLAB (The MathWorks, Inc.).

3.3. In Vivo Measurements

To demonstrate that the cTMS3 device generates electric field pulses that are sufficiently strong to produce cortical activation with various pulse parameter values, we determined active motor thresholds of the right first dorsal interosseous muscle for three pulse widths and two pulse polarities in ten healthy, right-handed volunteers (mean age = 29 ± 5 years, 5 women). The study was conducted at the Institute of Neurology, University College London and was approved by the National Research Ethics Service, UK.

The TMS coil was placed tangentially to the scalp with the short axis of the coil oriented at 45° from midline, approximately perpendicular to the central sulcus. Motor evoked potentials were recorded with electrodes in the belly–tendon montage connected to an electromiography amplifier. The coil position corresponding to maximum motor response (hot spot) was determined for pulses with posterior–anterior initial induced current direction in the brain (coil handle pointing backwards) by moving the coil in 0.5 cm steps around the hand motor area. The motor hot spot was checked for initial anterior–posterior current direction as well. When the hot spot was identified, the exact position was marked with a red pen on an elastic cap placed on the subject's head. The coil was held by hand in the same

position during the motor threshold assessment [31]. Active motor threshold was titrated while the subject was maintaining a 10% contraction of the target muscle. The pulse amplitudes were progressively reduced in 2% steps until a level was reached below which reliable electromyographic responses disappear [31]. The intervals between pulses were randomized. The active motor threshold was defined as the lowest pulse amplitude (voltage of V_{C11}) that evokes peak-to-peak motor potentials > 200 μV at least 5 out of 10 consecutive trials. The active motor threshold was determined with monophasic magnetic pulses for three pulse widths (30, 60, 120 μs) and two polarities (posterior–anterior and anterior–posterior initial induced current) in a pseudorandomized order. The pulse polarity was altered by changing the orientation of the TMS coil. These measurements were part of a larger study which included more extensive characterization of the TMS-evoked motor responses [22].

4. Experimental Results

4.1. Active Snubbing

Figure 2 demonstrates active snubbing of the ringing at the end of a TMS pulse. In this example, the pulse has positive monophasic current with peak value of I_L = 3 kA. As explained in Sec. 2.2, to provide a controllable effective resistance in parallel with the coil, Q_{12} is pulsed with a period of 5 μs and a duty ratio d. The duty ratio controls the effective output resistance of the IGBT, with resistance decreasing as d is increased. The dynamic response transitions from underdamped to overdamped for d above 0.625 – 0.65. For large duty ratios, corresponding to overdamped response, the electric field overshoot is small but the coil current has a relatively long decay and the energy is dissipated predominantly in the coil, potentially resulting in increased coil heating. On the other hand, for small duty ratios, corresponding to underdamped response, the coil current decays faster, but the electric field overshoot is larger and the electric field pulse tail exhibits ringing, with more heat dissipated in the IGBT modules due to their higher effective resistance. A trade-off between these two dynamic behaviors occurs near the critical damping duty ratio, d = 0.625 – 0.65, which is a good choice for the system design.

4.2. Motor Threshold vs. Pulse Width and Direction

Figure 3 demonstrates the use of cTMS3 to determine the strength–duration relationship between active motor threshold and pulse width in 10 subjects for two induced current directions: posterior–anterior and anterior–posterior. Figure 3(a) shows the electric field waveforms for the three pulses used in the study. The pulse width of the initial, positive electric field phase was set to 30, 60, or 120 μs. The initial amplitude of the subsequent negative electric field phase was 20% of the initial amplitude of the positive phase, V_{C21} = 0.2 V_{C11}. These pulses correspond to monophasic magnetic pulses with positive coil current, $I_L \geq 0$. Figure 3(b) shows the corresponding active motor thresholds. As expected, the motor threshold decreases with increasing pulse width and is lower for posterior–anterior than anterior–posterior current direction [15, 33]. The range of average threshold values in figure 3(b) is 572–1552 V, which is commensurate with the average active motor threshold of 37.3% of the maximum pulse amplitude, corresponding to energy-storage capacitor voltage of 1044 V, with a conventional monophasic TMS device (Magstim 200) [32].

4.3. Advanced Pulse Shape Synthesis

Figure 4 illustrates pulse synthesis with the four coil-voltage levels available in cTMS3. The initial energy-storage capacitor voltages are V_{C11} = 1430 V and $V_{C21} = 0.5\,V_{C11}$. The pulse starts with coil voltage steps of $-V_{C21}$, 0, $V_{11} - V_{C21}$, and V_{11}, and then goes through these steps is reverse order, forming an ascending and then descending staircase waveform of the electric field [figure 4 (b)]. This coil voltage waveform results in an approximately sine-shaped current pulse [figure 4 (a)]. Note that when $V_L \approx 0$ is applied across the coil, I_L is held at an approximately constant value near its peak or trough.

The transitions between the $V_L = 0$ and $V_L = V_{C11} - V_{C21}$ levels in figure 4 are associated with brief (1–3 μs) but relatively high amplitude electric field spikes. These coil voltage transitions correspond to simultaneous switching of both coil terminals, V_{x1} and V_{x2}. Therefore, sharp spikes in the coil voltage and hence the electric field can result from small differences in the switching speed of the two half-bridges. When simultaneous switching signals are sent to both half-bridges, differences in the speed of response of the respective IGBTs, which are different models with different specifications in the two half-bridges (see Table 1), result in slightly different timing of the voltage transitions of the coil terminals V_{x1} and V_{x2}. The resulting electric field transition spikes are too brief to significantly affect the neural membrane potential. Further, these spikes can be reduced or eliminated by optimizing the relative timing of the switch control signals, as discussed in the next paragraph and illustrated in figure 5.

The four electric field strength levels available within a pulse can be used to optimize various TMS performance aspects. For example, the energy efficiency of TMS pulses can be increased by introducing a long, shallow electric field phase that precedes the main, depolarizing pulse consisting of a positive and a negative rectangular phases of equal amplitudes [34]. Figure 5 illustrates how the cTMS3 device can be programmed to approximate this optimal pulse shape. The initial capacitor voltages were set to V_{C11} = 816 V and V_{C21} = 906 V. For the first 100 μs, the coil is connected between C_{21} to C_{11} resulting in initial coil voltage $V_L = V_{C11} - V_{C21} = -90$ V. During this initial negative phase, energy is transfered from C_{21} to C_{11}, resulting in approximately equal V_{C11} and V_{C21} at the end of the interval. The initial phase is followed by a bidirectional, near rectangular pulse; two different pulse durations are illustrated in figure 5. In this example, the electric field spike that could occur at the transition between the $V_L = 0$ and $V_L = V_{C11} - V_{C21}$ levels at the beginning of the pulse was avoided by delaying the Q_{21} turn-on signal by 1 μs relative to the Q_{11} turn-on signal.

4.4. Pulse Sequences and Repetitive TMS

The energy recycling, efficient rectangular electric field pulse shape, and pulse parameter control features of cTMS enable the generation of rapid pulse sequences that can approximate TMS paradigms that conventionally require the outputs of multiple devices to be combined. We provide two illustrative examples of paired-pulse [35] and quadripulse TMS [36] in figures 6 and 7, respectively. Both examples utilize two key cTMS capabilities: (1) generation of efficient biphasic magnetic pulses with different falling and rising slopes that induce an electric field with large difference between the amplitude of the positive and

negative pulse phases resulting in predominantly unidirectional electric field pulses, and (2) control of the effective stimulation strength of each pulse by adjusting the pulse width. The predominantly unidirectional electric field pulses approximate those generated by conventional monophasic stimulators but are substantially more energy efficient [14]. Increasing the pulse width of the second and subsequent pulses in a sequence can counteract the reduction of the capacitors' charge due to energy loss during the pulse, allowing the effective stimulation strength to be equal or even higher than that of the first pulse.

4.4.1. Paired-Pulse TMS—The paired-pulse example in figure 6 illustrates how the first (conditioning) pulse can be followed by a second (test) pulse of higher stimulation strength after only 3 ms. Capacitor voltages V_{C11} and V_{C21} were reduced after the first pulse by 2% and 17%, respectively. Nevertheless, by making the second pulse 67% longer than the first pulse, the effective strength of the second pulse, as quantified by the modeled neural membrane depolarization [figure 6(c)], is 45% higher than that of the first pulse.

4.4.2. Quardipulse TMS—Quadripulse rTMS involves bursts of unidirectional electric field pulses with interstimulus interval of 1.5–1250 ms that produces long-term-potentiation and long-term-depression effects [36]. Conventionally, quadripulse rTMS is generated by combining the output of four monophasic TMS devices [36]. Figure 7 demonstrates that a single cTMS device can generate a rapid quadripulse burst that uses small increments of the pulse width to compensate for the reduction of charge on the capacitors due to energy loss and the consequent reduction of pulse amplitude. Specifically, the duration of the second, depolarizing electric field phase is increased for each subsequent pulse, having values of 67, 69, 73, and 78 μs, respectively. Consequently, the estimated neural depolarization varied within only 1% across the pulses, whereas the reduction in the electric field amplitude was 16%. In practice, the adjustment of the pulse widths can also be based on empirical strength–duration curves like the ones in figure 3(b).

4.4.3. Theta Burst Stimulation—Another paradigm that requires rapid pulse sequences is theta burst stimulation which can induce lasting excitability changes after a relatively brief stimulus train [37]. The typical building block of theta burst stimulation is a 50 Hz burst of 3 pulses. Due to the high pulse rate, conventional theta burst stimulation uses bidirecitonal biphasic pulses. cTMS3 allows the generation of theta burst trains with a variety of pulse shapes including predominantly unidirectional electric fields. We evaluated the ability of cTMS3 to deliver theta bursts (50 Hz, 3 pulses) with predominantly unidirectional biphasic pulses similar to those in figures 6 and 7 with $V_{C11} = 1638\,V$, $V_{C21} = 0.2\,V_{C11}$, initial negative electric field phase width = 165 μs, and subsequent positive phase width = 45 μs. The measured pulse amplitude variability was within only 1.1%, indicating accurate pulse generation at 50 Hz. Experimental data from theta burst stimulation with these unidirecitonal pulses in humans is reported in [38].

5. Discussion

We demonstrated several implementation and functionality advantages of cTMS3. First, cTMS3 generates lower internal voltage differences compared to the cTMS2 device with nearly identical output ratings [14]. This contributes to the safety of the device. As well,

cTMS3 uses lower voltage IGBT modules that are less expensive and more available than the IGBT modules used in prior cTMS devices [13, 14], making this technology more practical for commercial implementation.

Second, cTMS3 enables more flexible pulse shaping by allowing two additional coil-voltage levels equal to zero or to the difference between the two energy-storage capacitor voltages, respectively. These additional voltage levels could be used to optimize the pulse shape for energy efficiency, as suggested by our theoretical findings [34]. We have demonstrated experimentally reduced energy use and coil heating with cTMS2 [14]—these advantages associated with the rectangular pulse shape and energy recycling should apply equally well to cTMS3. As well, the flexible pulse shaping could potentially improve the selectivity of neural population targeting [39, 40, 10], and mitigate TMS side effects such as the pulse sensation and sound [41, 16].

Third, the added zero coil-voltage level can be used to actively snub ringing between the capacitance at the switching nodes and the coil. Waveform ringing is a significant issue in other devices with enhanced pulse shape control such as flexTMS [17] and cTMS2 [14]. In flexTMS no measures were taken to suppress the ringing, whereas in cTMS2 active snubbing is handled with a separate circuit. In contrast, implementing the snubbing with the main IGBT modules in cTMS3 decreases the complexity and cost of the device, and increases reliability. Depending on the duty ratio of the IGBT switching during snubbing, various damping behaviors can be achieved, allowing optimization of the artifact suppression at the pulse end (see figure 2). IGBT active snubbing resulting in critical damping presents a favorable trade-off between suppressing the electric field pulse fast and with small overshoot, but having a long decay of the coil current resulting in more heat dissipation in coil, versus more overshoot and ringing associated with more heat dissipation in the IGBT modules. Importantly, this damping approach can be implemented in other topologies that allow a $V_L \approx 0$ level, such as the H-bridge used in flexTMS.

Fourth, due to its high energy efficiency, large capacitor energy storage, and pulse width and directionality control, cTMS3 can produce powerful rapid pulse sequences. Conventional TMS devices consisting of a single pulse-generation circuit cannot produce unidirectional theta burst stimulation or rapid bursts (< 10 ms inter-pulse interval) with equal or increasing strength, since capacitor energy diminishes from pulse to pulse due to circuit losses, and the time between the pulses is too short for the capacitor charger to replenish the charge. In contrast, cTMS3 enables paradigms including theta burst stimulation with predominantly unidirectional electric field pulses [38], as well as paired-pulse and quadripulse TMS with a single pulse-generation circuit. The ability to deliver high frequency trains of unidirectional pulses may be a particular advantage since it has been demonstrated that different directions of stimulation activate different populations of neurons in motor and visual areas of the cerebral cortex [42, 43]. Currently available repetitive stimulators only deliver bidirectional pulses, which activate mixed populations of neurons. Their effects are highly variable from one person to another, probably because of individual differences in the mix of neurons activated [44]. The ability to deliver unidirectional stimulation may therefore make the effects of stimulation more reproducible across the population.

Finally, in addition to technical aspects of the cTMS3 design and performance, this paper presented illustrative motor threshold strength–duration data from the first-in-human study with the device. These data demonstrated that with cTMS3, pulse parameters other than amplitude, such as the electric field pulse width and ratio between the positive and negative phases, can be controlled to affect the motor cortex response. They further showed that the device output is well within the strength required to produce cortical activation and is commensurate in strength with conventional devices that have less flexible output control.

6. Conclusion

We presented the design, implementation, and first-in-human experimental data of a novel TMS device, cTMS3, that offers implementation advantages and flexibility of pulse shaping unparalleled in other available TMS devices. cTMS3 generates smaller internal voltage differences and uses IGBTs with lower voltage rating than prior cTMS devices, provides additional coil voltage levels that are used to shape the pulse and to snub undesirable pulse ringing, and allows the generation of rapid sequences of pulses with various shapes and equal or even increasing strength that can implement various established and novel stimulation paradigms. These features enhance the potential of TMS as a research, diagnostic, and therapeutic tool.

Acknowledgments

This work was supported by grants from Rogue Research Inc., the NIH (R21EB006855), Columbia University Technology Ventures, Duke-Coulter Translational Partnership Grant Program, and the European Union (REPLACES: an FP7 Collaborative Project (222918)). A.V.P. is inventor on patents and patent applications on TMS technology assigned to Columbia University and Duke University, including cTMS technology licensed to Rogue Research, and has received patent royalties, research support, and travel support from Rogue Research through Columbia University and Duke University. J.C.R. has received loans of cTMS equipment from Rogue Research.

The authors thank Martin Sommer and Paul Hammond for assistance in collecting the data for figures 5(a), 3(a), and 7(a).

References

1. Peterchev AV, Wagner TA, Miranda PC, Nitsche MA, Paulus W, Lisanby SH, Pascual-Leone A, Bikson M. Fundamentals of transcranial electric and magnetic stimulation dose: Definition, selection, and reporting practices. Brain Stimul. 2012; 5:435–453. [PubMed: 22305345]
2. Heise K-F, Zimerman M, Hoppe J, Gerloff C, Wegscheider K, Hummel FC. The aging motor system as a model for plastic changes of GABA-mediated intracortical inhibition and their behavioral relevance. J Neurosci. 2013; 33:9039–9049. [PubMed: 23699515]
3. Quartarone A, Bagnato S, Rizzo V, Siebner HR, Dattola V, Scalfari A, Morgante F, Battaglia F, Romano M, Girlanda P. Abnormal associative plasticity of the human motor cortex in writer's cramp. Brain. 2003; 126:2586–2596. [PubMed: 14506068]
4. Sailer A, Molnar GF, Paradiso G, Gunraj CA, Lang AE, Chen R. Short and long latency afferent inhibition in Parkinson's disease. Brain. 2003; 126:1883–1894. [PubMed: 12805105]
5. O'Reardon JP, Solvason HB, Janicak PG, Sampson S, Isenberg KE, Nahas Z, McDonald WM, Avery D, Fitzgerald PB, Loo C, Demitrack MA, George MS, Sackeim HA. Efficacy and safety of transcranial magnetic stimulation in the acute treatment of major depression: a multisite randomized controlled trial. Biol Psych. 2007; 62(11):1208–1216.
6. Wassermann EM, Zimmermann T. Transcranial magnetic brain stimulation: Therapeutic promises and scientific gaps. Pharm Therapeutic. 2012; 133(1):98–107.

7. Hamada M, Ugawa Y, Tsuji S. High-frequency rTMS over the supplementary motor area for treatment of Parkinson's Disease. Mov Disord. 2008; 11:1524–1531. [PubMed: 18548577]
8. Lipton RB, Dodick DW, Silberstein SD, Saper JR, Aurora SK, Fischell RE, Ruppel PL, Goadsby PJ. Single-pulse transcranial magnetic stimulation for acute treatment of migraine with aura: a randomised, double-blind, parallel-group, sham-controlled trial. Lancet Neurol. 2010; 9:373–380. [PubMed: 20206581]
9. Jalinous, R. Principles of magnetic stimulator design. In: Pascual-Leone, A.; Davey, NJ.; Rothwell, J.; Wassermann, EM.; Puri, BK., editors. Handbook of Transcranial Magnetic Stimulation. London: Arnold; 2002. p. 30-38.
10. Sommer M, Alfaro A, Rummel M, Speck S, Lang N, Tings T, Paulus W. Half sine, monophasic and biphasic transcranial magnetic stimulation of the human motor cortex. Clin Neurophysiol. 2006; 117(4):838–844. [PubMed: 16495145]
11. Rothkegel H, Sommer M, Paulus W, Lang N. Impact of pulse duration in single pulse TMS. Clin Neurophysiol. 2010; 121(11):1915–1921. [PubMed: 20444645]
12. Barker AT, Garnham CW, Freeston IL. Magnetic nerve stimulation: the effect of waveform on efficiency, determination of neural membrane time constants and the measurement of stimulator output. Electroencephalogr Clin Neurophysiol Suppl. 1991; 43:227–237. [PubMed: 1773760]
13. Peterchev AV, Jalinous R, Lisanby SH. A transcranial magnetic stimulator inducing nearrectangular pulses with controllable pulse width (cTMS). IEEE Trans Biomed Eng. 2008; 55(1):257–266. [PubMed: 18232369]
14. Peterchev AV, Murphy DL, Lisanby SH. Repetitive transcranial magnetic stimulator with controllable pulse parameters. J Neural Eng. 2011; 8:13. 036016.
15. Peterchev AV, Goetz SM, Westin GG, Luber B, Lisanby SH. Pulse width dependence of motor threshold and input-output curve characterized with controllable pulse parameter transcranial magnetic stimulation. Clin Neurophysiol. 2013; 124:1364–1372. [PubMed: 23434439]
16. Goetz SM, Murphy DLK, Peterchev AV. Transcranial magnetic stimulation device with reduced acoustic noise. IEEE Mag Lett. 2014 in press.
17. Gattinger N, Moessnang G, Gleich B. flexTMSA novel repetitive transcranial magnetic stimulation device with freely programmable stimulus currents. IEEE Trans Biomed Eng. 2012; 59(7):1962–1970. [PubMed: 22531742]
18. Basham E, Yang Z, Liu W. Circuit and coil design for in-vitro magnetic neural stimulation systems. IEEE Trans Biomed Circ Sys. 2009; 3(5):321–331.
19. Goetz, SM.; Pfaeffl, M.; Huber, J.; Singer, M.; Marquardt, R.; Weyh, T. Circuit topology and control principle for a first magnetic stimulator with fully controllable waveform. ; Proc IEEE Eng Med Biol Conf; 2012. p. 4700-4703.
20. Peterchev, AV. Circuit topology comparison and design analysis for controllable pulse parameter transcranial magnetic stimulators; Proc IEEE EMBS Neural Eng Conf; 2011. p. 646-649.
21. Peterchev, AV.; Murphy, DL. Controllable pulse parameter transcranial magnetic stimulator with enhanced pulse shaping; Proc IEEE EMBS Neural Eng Conf; 2013. p. 121-124.
22. D'Ostilio, K.; Goetz, S.; Ciocca, M.; Chieffo, R.; Chen, J-CA.; Peterchev, AV.; Rothwell, JC. Effect of coil orientation on strength-duration time constant with controllable pulse parameter transcranial magnetic stimulation. Clin Neurophysiol; Abstracts from 30th International Congress of Clinical Neurophysiology; 2014. (in press)
23. Giesselmann, M.; Palmer, B.; Neuber, A.; Donlon, J. High voltage impulse generator using HV-IGBTs; Proc IEEE Int Pulsed Power Conf; 2005. p. 763-766.
24. Petterteig, A.; Lode, J.; Undeland, TM. IGBT turn-off losses for hard switching and with capacitive snubbers; Rec IEEE Ind App Soc Ann Mtg; 1991. p. 1501-1507.
25. Trivedi M, Shenai K. Modeling the turn-off of IGBT's in hard- and soft-switching applications. IEEE Trans Electron Dev. 1997; 44(5):887–893.
26. Severns, R. Snubber Circuits for Power Electronics. SMPS Technology; 2008. [E-book] Available: http://www.snubberdesign.com/snubber-book.html.
27. Ray, WF.; Hewson, CR. High performance Rogowski current transducers; Conf Rec IEEE Ind App Conf; 2000. p. 3083-3090.

28. Oates, CDM.; Burnett, AJ.; James, C. The design of high performance Rogowski coils; Int Conf Power Electron Machines Drives; 2002. p. 568-573.
29. Corthout E, Barker AT, Cowey A. Transcranial magnetic stimulation: Which part of the current waveform causes the stimulation? Exp Brain Res. 2001; 141(1):128–132. [PubMed: 11685417]
30. Lapicque L. Recherches quantitatives sur lexcitation lectrique des nerfs traite comme une polarisation. J Physiol Pathol Gen. 1907; 9:620–635.
31. Rothwell JC, Hallett M, Berardelli A, Eisen A, Rossini P, Paulus W. Magnetic stimulation: motor evoked potentials. Electroencephalogr Clin Neurophysiol. 1999; (Suppl 52):97–103.
32. Oliviero A, Profice P, Tonali PA, Pilato F, Saturno E, Dileone M, Ranieri F, Di Lazzaro V. Effects of aging on motor cortex excitability. Neurosci Res. 2006; 55:74–77. [PubMed: 16584795]
33. Niehaus L, Meyer B-U, Weyh T. Influence of pulse configuration and direction of coil current on excitatory effects of magnetic motor cortex and nerve stimulation. Clin Neurophysiol. 2000; 111:75–80. [PubMed: 10656513]
34. Goetz SM, Truong NC, Gerhofer MG, Peterchev AV, Herzog H-G, Weyh T. Analysis and optimization of pulse dynamics for magnetic stimulation. PLOS ONE. 2013; 8(3):e55771, 12. [PubMed: 23469168]
35. Ziemann, U. Paired pulse techniques. In: Pascual-Leone, A.; Davey, NJ.; Rothwell, J.; Wassermann, EM.; Puri, BK., editors. Handbook of Transcranial Magnetic Stimulation. London: Arnold; 2002. p. 141-163.
36. Hamada M, Terao Y, Hanajima R, Shirota Y, Nakatani-Enomoto S, Furubayashi T, Matsumoto H, Ugawa Y. Bidirectional long-term motor cortical plasticity and metaplasticity induced by quadripulse transcranial magnetic stimulation. J Physiol-London. 2008 Aug 15; 586(16):3927–3947. [PubMed: 18599542]
37. Huang YZ, Edwards MJ, Rounis E, Bhatia KP, Rothwell JC. Theta burst stimulation of the human motor cortex. Neuron. 2005; 45(2):201–206. [PubMed: 15664172]
38. Hannah, R.; Ciocca, M.; Sommer, M.; Hammond, P.; Rothwell, JC. Continuous theta burst stimulation with monophasic pulses: effect of current direction. Clin Neurophysiol; Abstracts from 30th International Congress of Clinical Neurophysiology; 2014. (in press)
39. McIntyre CC, Grill WM. Selective microstimulation of central nervous system neurons. Ann Biomed Eng. 2000; 28(3):219–233. [PubMed: 10784087]
40. McIntyre CC, Grill WM. Extracellular stimulation of central neurons: Influence of stimulus waveform and frequency on neuronal output. J Neurophysiol. 2002; 88(4):1592–1604. [PubMed: 12364490]
41. Geddes LA. Optimal stimulus duration for extracranial cortical stimulation. Neurosurgery. 1987; 20(1):94–99. [PubMed: 3808283]
42. Day BL, Dressler D, Maertens de Noordhout A, Marsden CD, Nakashima K, Rothwell JC, Thompson PD. Electric and magnetic stimulation of human motor cortex: surface EMG and single motor unit responses. J Physiol. 1989; 412:449–473. [PubMed: 2489409]
43. Kammer T, Beck S, Erb M, Grodd W. The influence of current direction on phosphene thresholds evoked by transcranial magnetic stimulation. Clin Neurophysiol. 2001; 112(11):2015–2021. [PubMed: 11682339]
44. Hamada M, Murase N, Hasan A, Balaratnam M, Rothwell JC. The role of interneuron networks in driving human motor cortical plasticity. Cereb Cortex. 2013; 23(7):1593–1605. [PubMed: 22661405]

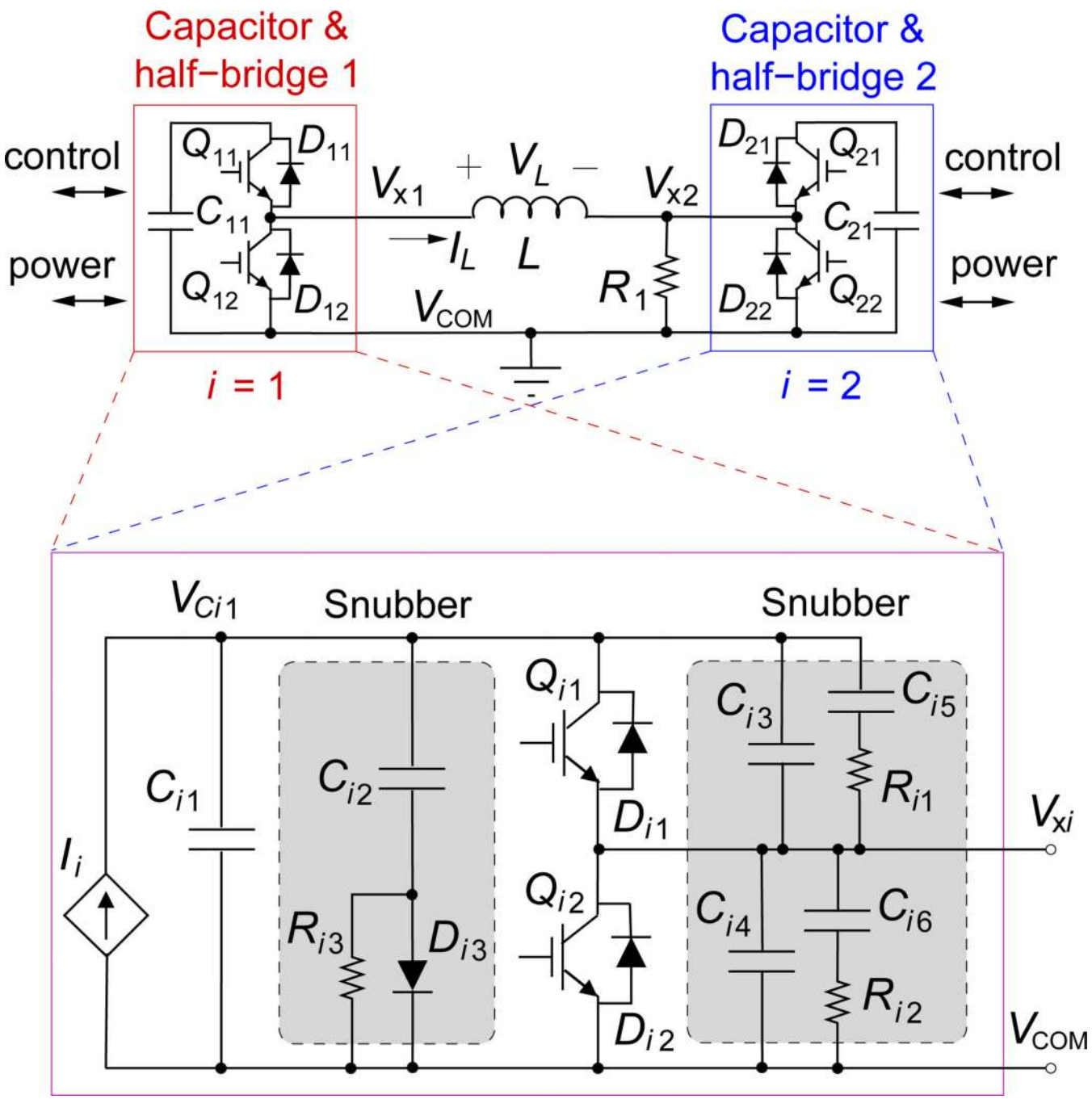

Figure 1.

Diagram of key elements of the cTMS3 circuit. (top) Two half-bridges connected to energy storage capacitors (i = 1,2) drive differentially the stimulation coil L. (bottom) Each half-bridge, $Q_{i1}/D_{i1} - Q_{i2}/D_{i2}$, is connected to an energy-storage capacitor C_{i1} and charge control module I_i. Passive snubber circuits are shown in shaded blocks.

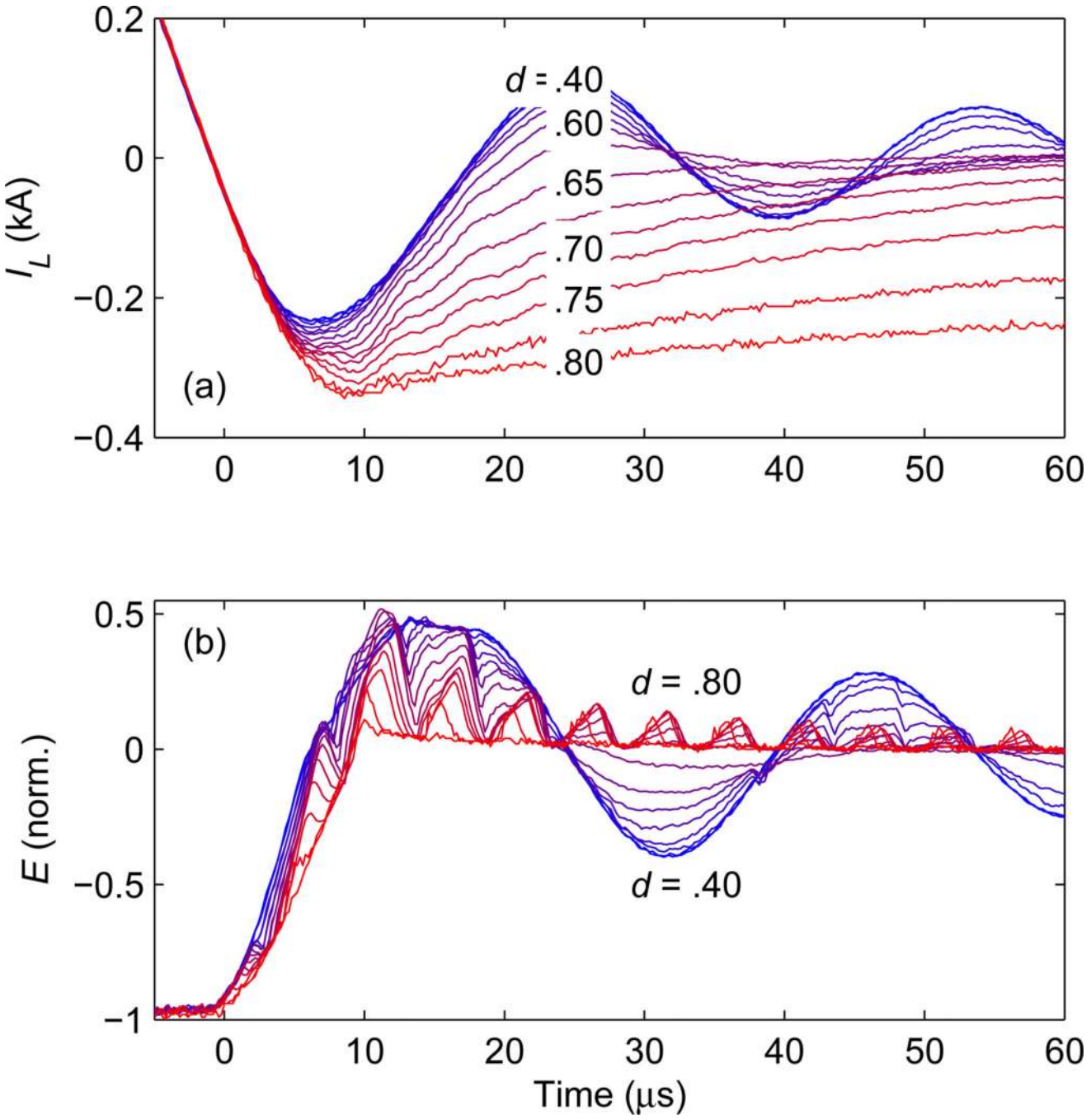

Figure 2.

Measured active snubbing at the end of a positive monophasic TMS pulse with peak coil current of I_L = 3 kA. Ideally, I_L should decay to zero and remain there. However, ringing occurs between the coil and the switch capacitive snubbers. To dampen these oscillations, transistor Q_{12} is switched with a period of 5 μs and various duty ratios *d*. (a) Coil current I_L and (b) corresponding induced electric field strength *E* are shown for a *d* range of 0.4–0.8 [*d* values printed over the traces in (a)]. For $d > 0.625$, the response transitions from underdamped to overdamped.

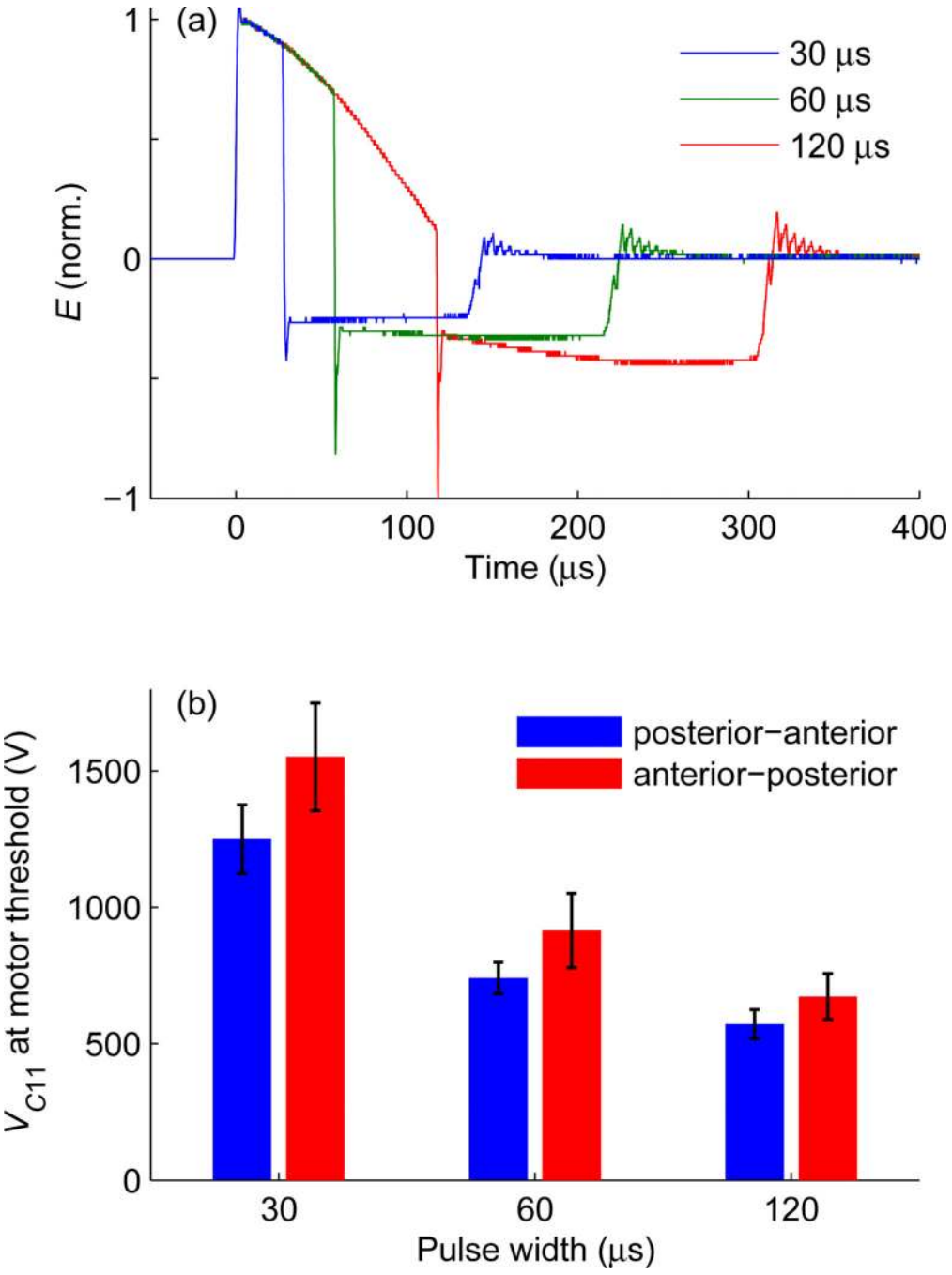

Figure 3.

Motor threshold measurement in 10 human subjects as a function of pulse width and current direction. (a) Measured electric field waveform E of monophasic magnetic pulses with $V_{C21} = 0.2\,V_{C11}$ and positive phase widths of 30, 60, and 120 µs. (b) Active motor thresholds for the three pulse widths with posterior–anterior and anterior–posterior direction of the initial phase of the induced current. Bars give mean values and whiskers give standard deviation. For comparison, the active motor threshold with a conventional monophasic TMS device (Magstim 200) is 1044±252 V [32].

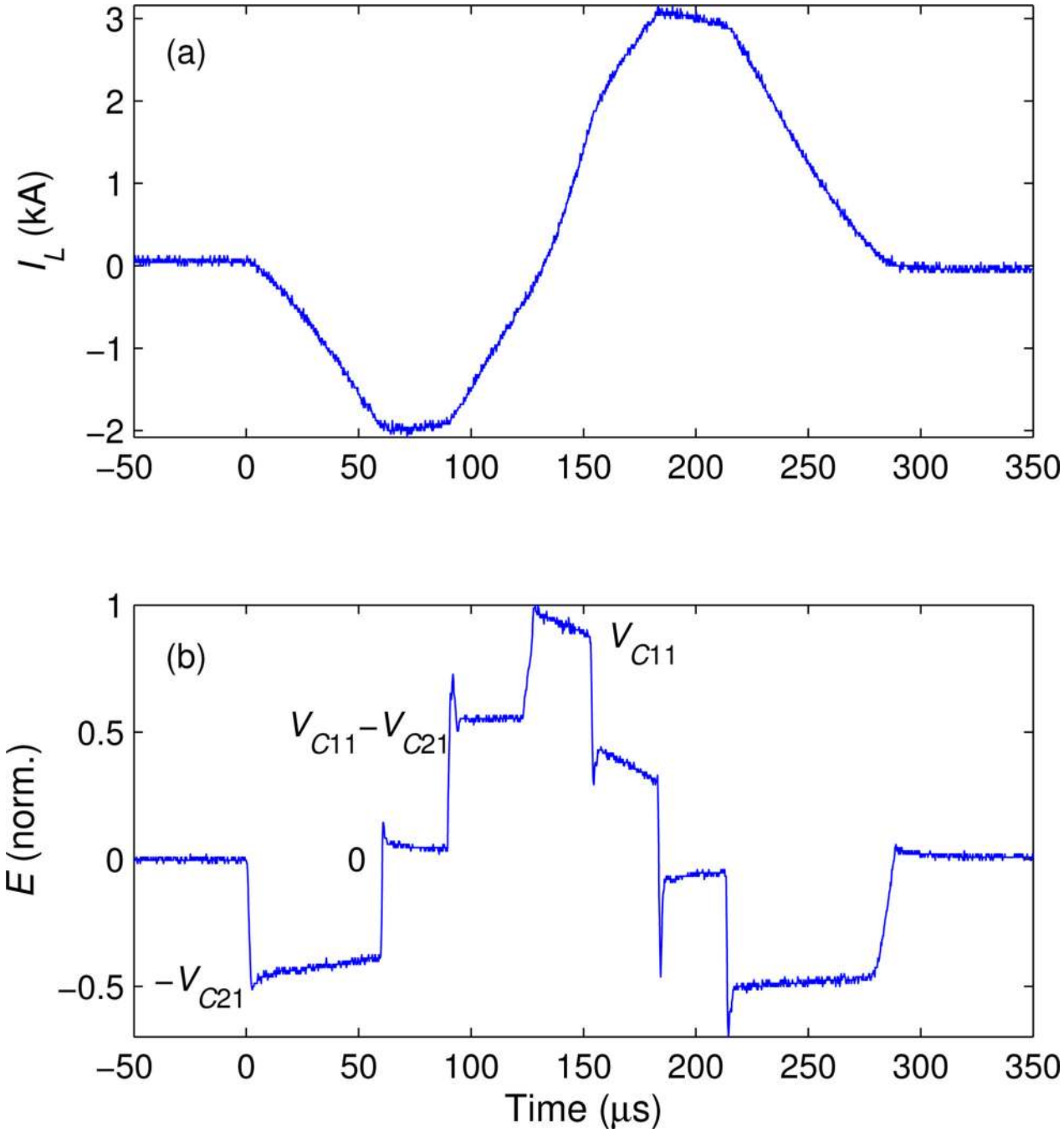

Figure 4.

Measured waveforms of (a) coil current I_L and (b) electric field E for a synthesized staircase pulse illustrating the four E levels that can be achieved within each pulse. Coil voltages corresponding to each E level are indicated in (b). Initial energy-storage capacitor voltages are V_{C11} = 1430 V and $V_{C21} = 0.5\,V_{C11}$.

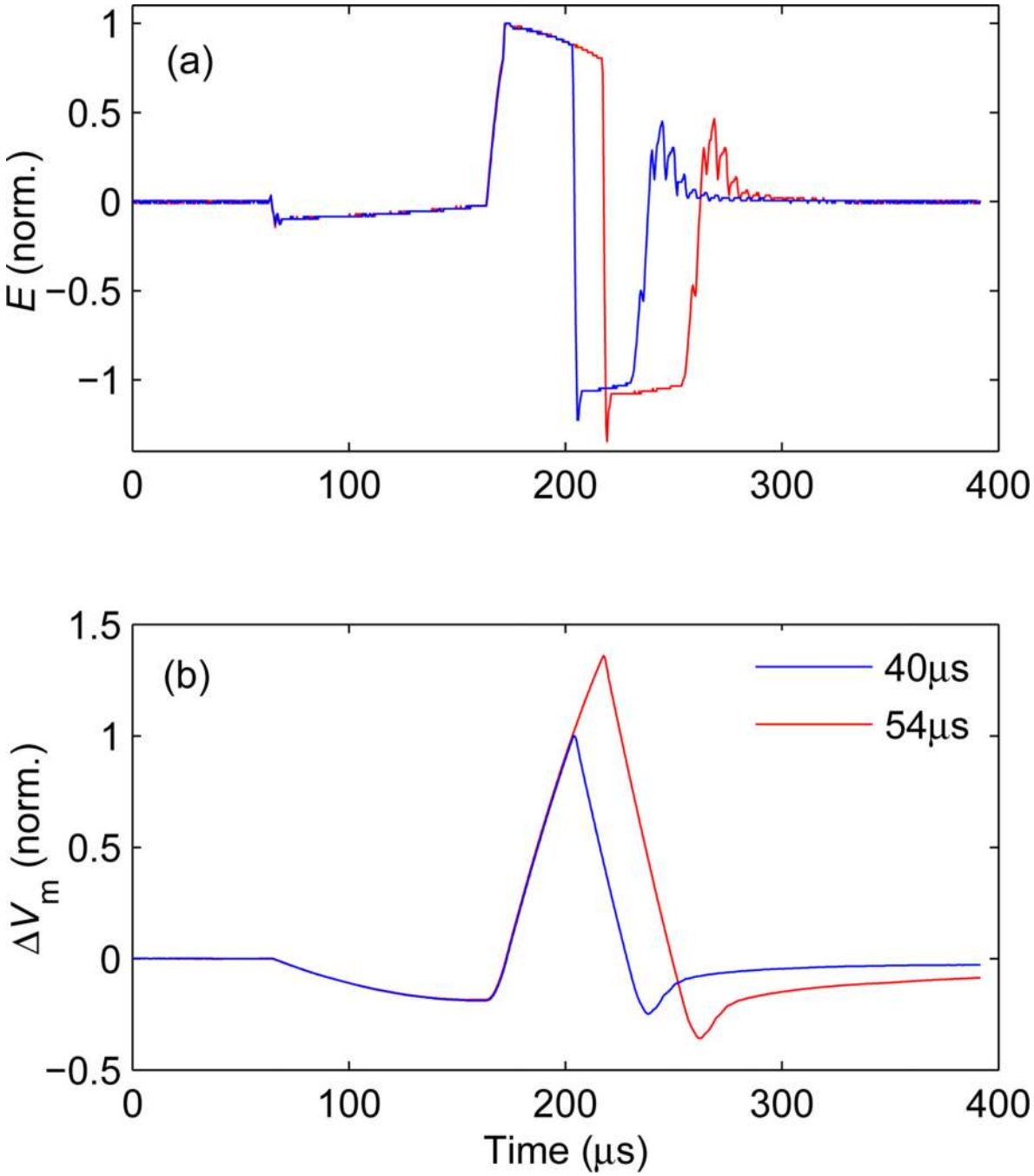

Figure 5.

(a) Measured electric field waveform E and (b) estimated neural membrane depolarization ΔV_m for a pulse approximating minimum energy pulses [34]. The initial capacitor voltages are V_{C11} = 816 V and $V_{C21} = 1.1\,V_{C11}$. The duration of the initial negative E phase is 100 µs and the width of the second, positive phase is either 40 µs (blue curves) or 54 µs (red curves).

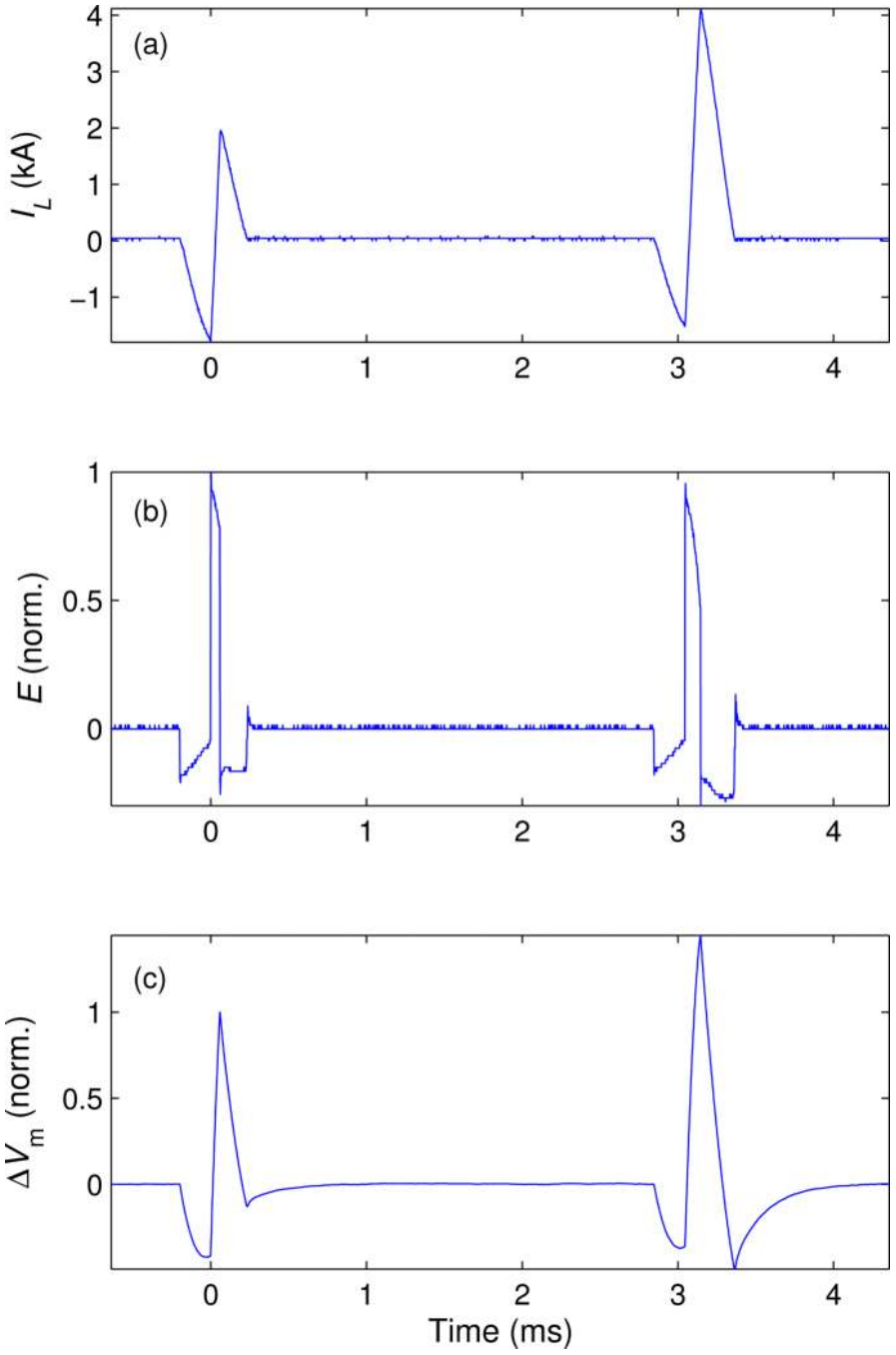

Figure 6.

Pair of biphasic pulses delivered with short interstimulus interval (3 ms). The plots show measurements of (a) coil current I_L and (b) electric field E, as well as (c) modeled neural membrane depolarization ΔV_m. The parameters of the first pulse are V_{C11} = 1196 V, V_{C21} = 0.22 V_{C11}, and positive E phase width of 60 μs. In the second pulse, the positive E phase width is increased to 100 μs, resulting in larger membrane depolarization despite the reduced E amplitude.

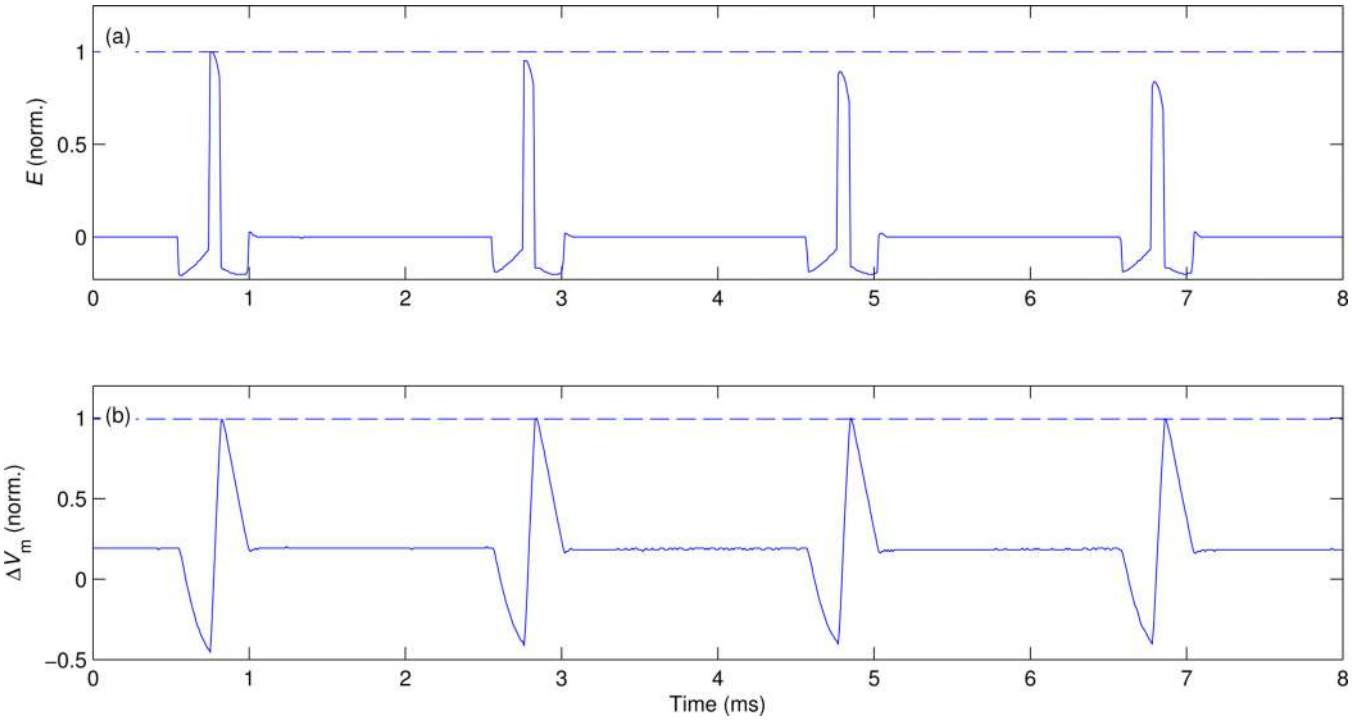

Figure 7.

Four pulses separated by inter stimulus interval of 2 ms forming a quadripulse burst [36]. The plots show (a) measured electric field waveform E (filtered with 3-point median filter to illustrate clearly pulse amplitude by removing switching spikes) and (b) estimated neural membrane depolarization ΔV_m. The initial capacitor voltages are V_{C11} = 1230 V and V_{C21} =0.22 V_{C11}, and the duration of the first, negative phase of the electric field pulses is fixed at 200 μs. In order to compensate for the reduction of charge on the capacitors due to energy loss and the consequent reduction of pulse amplitude, the duration of the second, positive electric field phase is increased for each subsequent pulse, having values of 67, 69, 73, and 78 μs, respectively.

Table 1

Key cTMS3 Circuit Implementation Components

Component	Function	Rating	Part #	Manufacturer
C_{11}	energy storage	430 μF, polypropylene film	700D437930-556[a]	SB Electronics
C_{21}	energy storage	2000 μF, polypropylene film	700D208915-555[a]	SB Electronics
Q_{11}/D_{11}, Q_{12}/D_{12}	coil switch	IGBT: 1200 Adc, 3.3 kV	5SNA1200E330100	ABB
Q_{21}/D_{21}, Q_{22}/D_{22}	coil switch	IGBT: 1200 Adc, 1.7 kV	FZ1200R17HP4	Infineon
Q_{11}, Q_{12}, Q_{21}, Q_{22} gate drivers	gate drivers	$V_{GE} = -10$ V (off), 20 V (on) $R_G = 1$ Ω (off), 11 Ω (on)	HV4-30I[a]	Floeth Electronic
L	stimul. coil	16.35 μH	P/N 9925-00[a]	Magstim
C_{12}	snubber	2.4 μF, polyester film	(3) 45PC804928-117[a]	SB Electronics
R_{13}	snubber	0.66 Ω, non-inductive	(3) NHL-20-02Z	Vishay Dale
C_{22}	snubber	6 μF, polyester film	(3) 45PC205915-116[a]	SB Electronics
R_{23}	snubber	0.33 Ω, non-inductive	(3) MRA121R000FE12	Vishay Dale
D_{13}, D_{23}	snubber	1200 V, 60 A, fast recovery	(3) 60EPF12	Vishay Semi.
C_{13}, C_{14}, C_{23}, C_{24}	snubber	0.5 μF, polyesther film	45PC113[a]	SB Electronics
C_{15}, C_{16}, C_{25}, C_{26}	snubber	1 μF, polyesther film	(2) 45PC113[a]	SB Electronics
R_{11}, R_{12}, R_{21}, R_{22}	snubber	0.5 Ω, non-inductive	(4) NHL-25-06Z 2 Ω	Vishay Dale
R_1	coil grounding	100 kΩ	(4) HVR37 100 kΩ	Vishay BC Comp.
I_1	cap. charger	output: 3 kV, 0.67 A, 1 kW	102A-3KV-POS	Lambda
I_2	cap. charger	output: 1.5 kV, 1.33 A, 1 kW	102A-1.5KV-POS	Lambda
control	digital controller	digital I/O 0.025 μs resol. 12 bit A/D, 16 bit D/A	cRIO-9014 + modules: 9401, 9403, 9201, 9263	National Instrum.

[a] custom manufactured or modified